Robotic complex for inspection of the outer surface of the aircraft in its parking lot

Boris S. ALESHIN[1], Alexander I. CHERNOMORSKY*[,1], Eduard D. KURIS[1], Konstantin S. LELKOV[1], Maxim V. IVAKIN[1]

*Corresponding author
[1]Department of Automated Complexes of Orientation and Navigation Systems, Moscow Aviation Institute (National Research University), 4 Volokolamskoe Shosse, 125993, Moscow, Russian Federation, chernomorscky@yandex.ru*, ekuris@mail.ru, kon.lelkov@gmail.com, ivakin.maksim2@gmail.com

DOI: 10.13111/2066-8201.2020.12.S.2

Received: 12 March 2020/ Accepted: 30 May 2020/ Published: July 2020

Abstract: *Through-flight inspection of the outer surface of the aircraft is necessary to identify possible damage to the surface of the aircraft caused by metal fatigue, lightning, birds collision, etc. The article discusses the method of robotic inspection of the outer surface of the aircraft in its open air parking area. The robotic complex (RC) consists of an unmanned ground vehicle (UGV) and an unmanned aerial vehicle (UAV) interconnected by a tether mechanism (TM). The algorithm of the RC functioning is presented. The main attention is paid to the formation of the TM control and the features of its work, ensuring the prevention of collisions of UAV with aircraft during extreme wind actions on UAV. The study of the most critical mode of the complex operation under extreme wind actions on an unmanned aerial vehicle is carried out. The results of modeling the typical process of the RC operation in an abnormal conditions of extreme wind exposure to UAV are presented.*

Key Words: *unmanned aerial vehicle, unmanned ground vehicle, tether mechanism, mathematical model, wind action, modeling*

1. INTRODUCTION

Through-flight inspection of the outer surface of the aircraft is a mandatory procedure. It is carried out by engineering and technical personnel along a route pre-established by the regulations [1], [2]. The main disadvantages of this approach to the inspection procedure are the significant time and material work efforts, as well as the significant influence of the human factor on the identification and assessment of the characteristics of detected defects on the outer surface of the aircraft. In [3], a variant of automated inspection of the outer surface of the aircraft with the help of a robot camera moving on the surface of the aircraft and held on it by a special suction cup system is considered. An obvious drawback of this approach is the relatively long inspection procedure.

In recent years, a number of companies began to use multi-rotor UAVs to inspect the outer surface of aircraft. So, the Airbus group company has developed a UAV that can be used to inspect the upper part of the outer surface of the aircraft, but only in the hangar, because free flights of UAVs in the airspace of the airfield are prohibited by the regulations [4]. The images received from the camera located on the UAV during its movement along a given route are analyzed in the computer of the ground control unit. The use of UAV makes it possible to accurately position and determine the parameters of damage to the aircraft surface. A similar approach to the inspection of the outer surface of the aircraft is being developed by ST Engineering Air NZ [5]. At the same time, this company is making attempts to change the inspection schedule in order to use UAV free flight at open aircraft parking areas, which seems problematic. According to the developers, the time of inspection of the outer surface of the aircraft is reduced from six to two hours. In both cases, inspection of the lower part of the outer surface of the aircraft is carried out by engineering and technical personnel. The possibility of monitoring the entire outer surface of the aircraft with the UAV is indicated in [6], however, the use of this approach is practically impossible, in particular, with a low location of aircraft engines.

To solve the tasks of comprehensive monitoring of objects of the surrounding space, in a number of works it was proposed to use UAV together with UGV as part of the RC. With the help of such RCs, simultaneous monitoring is carried out by cameras mounted on both UAV and UGV [7], [8], [9], [10], [11], [12]. In a number of RC implementation variants, the UAV is connected to the UGV with a tether, which can be used both to provide the UAV with power from the UGV and to keep the UAV from drift during large wind actions [13], [14], [15], [16].

The robotic complex, consisting of UGV and UAV connected by a tether mechanism, is undoubtedly promising for the purpose of monitoring the entire outer surface of the aircraft in its open air parking area. When using such a RC for inspection of the aircraft surface, a critical factor is the operation of the TM, which guarantees the elimination of collisions between UAV and aircraft in conditions of extreme wind actions on UAV.

The purpose of this work is to describe the method of robotic through-flight (predeparture) inspection of the outer surface of the aircraft in its open air parking area. The robotic complex used consists of UGV and UAV connected by a tether mechanism. The main attention is paid to the formation of the TM control and the features of its work, ensuring the prevention of collisions of UAVs with aircraft during extreme wind actions on UAVs.

2. ALGORITHM FOR FUNCTIONING A ROBOTIC COMPLEX WITH A CORD MECHANISM

RC works as follows. Initially, the UGV with the UAV located on its landing place is in the base. According to the signal from the ground control unit to the UGV, the UGV travels from the UAV to the aircraft parking area at the turning point A of the S and T UGV trajectories. Then, the UAV takes off to a point B in its trajectory R with simultaneous regulation of the length l_t of the tether segment connecting the UAV with the UGV. This regulation in the normal mode both during take-off and in the subsequent flight along the trajectory R, as well as during UAV landing on the UGV, is carried out so that, on the one hand, the length of this tether segment slightly exceeds the current distance between the UAV and UGV, and on the other hand does not exceed the value at which the UAV under the influence of random external disturbances, in particular wind, can collide with the surface of the aircraft.

With such a length of the connecting segment of the tether, it is possible to exclude its tension, to exclude the force impact of the tether on the UAV and, therefore, to disrupt the normal operation of its camera. Next, the UAV is flying under the control of its autopilot from point B along the trajectory R with returning to this point while photographing all the elements of the upper part of the outer surface of the aircraft in accordance with its three-dimensional model. At the same time, according to the specified program, the rotational orientation of the UAV camera installed in the gyrostabilized three-degree-of-freedom suspension is controlled.

The trajectory S, along which the UGV, under the control of its autopilot, accompanies the UAV, is essentially a projection of the trajectory R onto the surface of the aircraft parking area. After the synchronous return of the UAV to point B and UGV to point A, the UAV lands at the UGV landing place. Upon completion of the UAV landing, the UGV moves along the trajectory T from point A with a return to this point while photographing all the elements of the lower part of the outer surface of the aircraft in accordance with its three-dimensional model. The accident-free passage of the UGV is supported by its system for detecting and avoiding obstacles [17], [18].

At the same time, according to a predetermined program, the rotational orientation of the UGV camera, also installed in a gyrostabilized three-degree-of-freedom suspension, is controlled. Upon the return of the UGV from the UAV to point A, the photographs, linear and angular coordinates of the UAV and UGV, as well as the rotational orientation parameters of their cameras relative to the UAV and UGV, respectively, are transferred to the ground control unit computer. This computer implements the analysis of photographs with the determination of the coordinates of the location, nature and parameters of damage to both the lower and upper parts of the outer surface of the aircraft. Then UGV with UAV returns to the base. Figure 1 shows a diagram illustrating the functioning of the RC during inspection of the outer surface of the aircraft in its open air parking area.

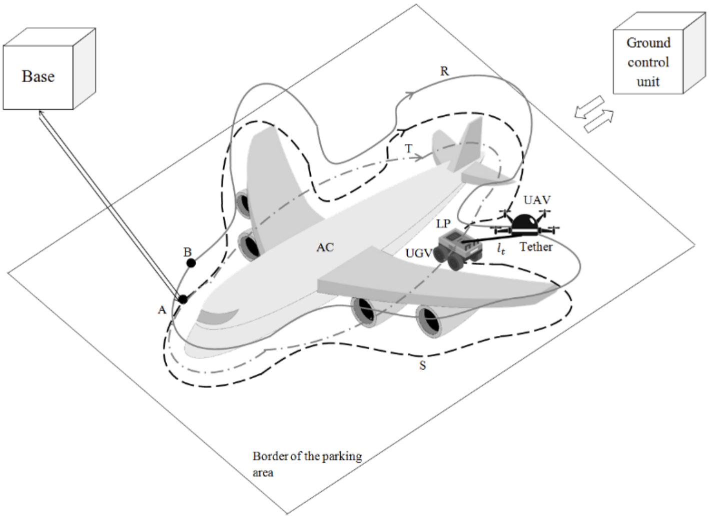

Fig. 1 – Diagram illustrating the functioning algorithm of the robotic complex

Figure 1 indicates: the border of the aircraft parking area; the actual aircraft; robotic complex, including UAV (such as a quadrocopter) with cameras, UGV with cameras, tether mechanism connecting the UAV with UGV; ground control unit; base of UGV with UAV; l_t is the current length of the adjustable cord segment, landing place (LP) of the UAV in the UGV; R – UAV trajectory for inspection of the upper part of the outer surface of the aircraft; S and T, respectively, are the trajectory along which the UGV accompanies the UAV, and the UGV trajectory for inspection of the lower part of the outer surface of the aircraft. The location parameters of the trajectory R of UAV, S and T UGV trajectories, program for changing the rotational orientation of the UAV and UGV cameras during inspection are set based on the use of information about the type of aircraft being inspected.

One of the most important operating modes of the RC is its abnormal mode in extreme conditions of external influences, in particular wind. In the normal operation, the aerodynamic force of the wind action on the UAV is corrected by the thrust forces developed by the UAV propellers when it is tilted, generally in roll and pitch. In abnormal conditions, to correct the wind aerodynamic force of the thrust forces of the propellers is not enough and it is necessary to use a controlled tether mechanism.

This mechanism, for example, may contain a coil with a tether wound around it, mounted on the output shaft of a DC motor; the motor, in turn, is installed on board the UGV. The end of the tether is fixed on board the UAV. With a small dead weight of the tether (made, for example, of fiberglass), we can assume that the processes of unwinding and winding the tether to the coil are carried out under the action of forces applied to it both from the UAV and from the TM drive motor. TM control is carried out by forming a control voltage supplied to the corresponding winding of the drive motor.

First, we determine the functional algorithm for the formation of this voltage in the most critical situation when the wind load on the UAV is directed normal to its trajectory in the direction of the portion of the outer surface of the aircraft, next to which the UAV is at the current time. We assume that when an emergency occurs, the UGV stops; while the autopilot levels and holds the UAV at the nominal altitude and heading angle. A diagram illustrating in this case the distribution of forces applied to the UAV while holding it with the help of the TM is presented in Figure 2.

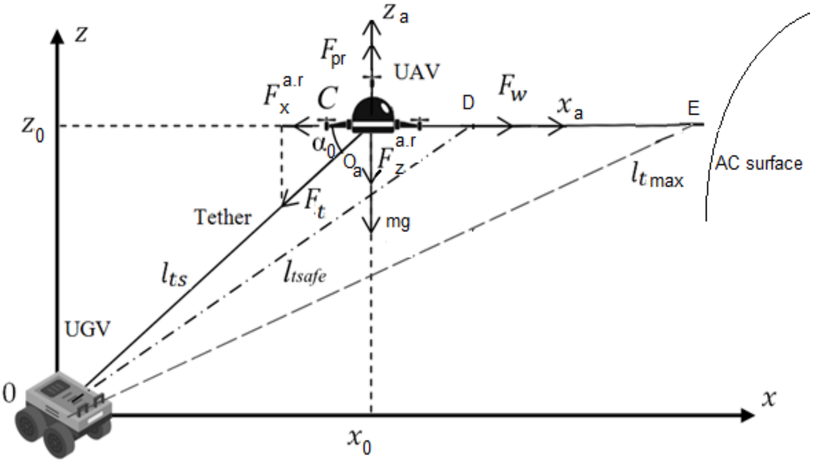

Fig. 2 – Distribution of forces applied to the UAV

This figure indicates: $O_a x_a z_a$ is the system of coordinates (SC), rigidly connected with the UAV (O_a is the center of mass (CM) of the UAV, the axis $O_a x_a$ is horizontal and normal to the UAV trajectory in the side of the outer surface of the aircraft, the axis $O_a z_a$ is directed vertically); Oxz is the SC with the center O in the UGV center of mass (its axes are parallel to the corresponding axes of the SC $O_a x_a z_a$); C is the starting point at which the UAV is in front of a gust of wind (its coordinates are x_0, z_0); D, E are the UAV location points at which the control voltage of the TM drive motor is switched; l_{ts}, l_{tsafe}, l_{tmax} are the lengths of the tether segments from the UGV to the UAV at its location, respectively, at points C, D, E; F_w is the aerodynamic force created by the wind load on the UAV; F_t is the force acting on the UAV from the side of the tether; F_{pr} is the thrust force generated by propellers [19]; mg is the UAV gravity ($m -$ UAV mass, $g -$ gravity acceleration) ; $F_x^{a.r.}, F_z^{a.r.}$ are the aerodynamic drag forces, respectively, along the axes x_a , z_a; α_0 is the tether tilt angle relative to the horizon plane when the UAV is located at point C.

Immediately before the emergency operation, in accordance with Figure 2, the UAV is at point C, the tether length is l_{ts}, and the control voltage U is absent on the drive motor. In abnormal conditions, the entire TM operation cycle can be represented as a combination of several successive phases. In the first phase, under the influence of the aerodynamic force F_w, the UAV moves toward the surface of the aircraft, the tether is unwound, the control voltage U on the drive motor is still absent. When the tether reaches a certain threshold length l_{tsafe}, the first phase of the emergency mode of the TM ends (point D, Fig. 2). The second phase begins, at the beginning of which the control voltage of the maximum value $U = U_{max}$ enters the TM motor winding. The motor develops a moment that forms the force F_t on the tether. Under the action of the force determined by the sum of the projection onto the axis $O_a x_a$ of the force F_t ($F_t cos\alpha$), the force F_w and the force $F_x^{a.r.}$, the UAV loses speed in the direction of the axis $O_a x_a$.

At the time when this speed becomes equal to zero, the second phase of the cycle ends (point E, Fig. 2); in this case, the unwinding speed of the tether becomes equal to zero, and its length reaches the maximum value l_{tmax}. Then, at the beginning of the third phase of the cycle, the voltage U abruptly drops to an intermediate value U_{in}, at which the force $F_t cos\alpha$ is such that the UAV will move in the direction from the surface of the aircraft, increasing speed rather slowly. When the tether reaches the length l_{tsafe} (UAV – in point D, Fig. 2), the third phase of the cycle is completed. In the fourth phase, the voltage U is formed so that, under the prevailing influence of F_t, the UAV without significant overshoot along the x coordinate will return to the same position that it occupied before the emergency operation (point C, Fig. 2). In the fifth phase, the voltage U is formed in such a way as to ensure aperiodic attraction of the UAV to the UGV landing place.

3. MATHEMATICAL MODEL OF A ROBOTIC COMPLEX WITH A TETHER MECHANISM

Due to the forced stop of the UGV at point O (Fig. 2) and keeping it at this point, the equations of motion of the UGV in the mathematical model of the RC for the abnormal conditions can be omitted. By virtue of the assumptions made, the general mathematical model of the RC in these conditions can be considered as a combination of the motion model of the UAV's center of mass in the xz plane and the mathematical model of the TM [19], [20], [21], [22], [23], [24].

The mathematical model of the UAV:

$$m\ddot{x} = F_w - F_t cos\alpha - F_x^{a.r.}, \tag{1}$$

$$m\ddot{z} = F_{pr} - F_t sin\alpha - F_z^{a.r.} - mg, \tag{2}$$

$$\alpha = \arccos\frac{\mathrm{x}}{\sqrt{x^2 + z^2}}, \tag{3}$$

where x, are the coordinates of the UAV's center of mass in the Oxz SC; α is the current tether angle of inclination relative to the horizon plane. The aerodynamic drag forces $F_x^{a.r.}, F_z^{a.r.}$, directed by the velocity of the incoming air flow, are determined by the relations:

$$F_i^{a.r.} = c_{di}\frac{\rho v_i^2}{2}S_i, i = x, z \tag{4}$$

where c_{di}, v_i are dimensionless aerodynamic coefficients and free-stream velocities in the direction of the corresponding axes; S_i are effective surface area of the UAV, normal to the respective axes; ρ is the atmospheric density.

The mathematical model of TM with a DC motor:

$$L_c\dot{I} + R_cI = U - c_{cef}\omega_c, \tag{5}$$

$$(\mathcal{J} + mr_c{}^2)\dot{\omega_c} + \mathcal{E}\omega_c = M_{met} - ((F_wcos\alpha - F_x^{a.r.})cos\alpha + (F_{pr} - mg)sin\alpha)r_c, \tag{6}$$

$$M_{met} = nI;\ F_t = \frac{M_{met}I}{r_c}, \tag{7}$$

$$l_t = l_{ts} - r_c\int_0^t \omega_c dt, \tag{8}$$

where U is the control voltage on the motor; I is the current in the drive winding of the motor; ω_c is the rotational speed of the motor shaft with the coil ($\omega_c > 0$ when winding the tether onto the coil); M_{met} is the electromagnetic torque on the motor shaft; $\mathcal{J}$ is the inertia moment to motor shaft with a coil; $\mathcal{E}$ is the coefficient of viscous friction moment about the axis of rotation of the motor shaft; L_c, R_c – respectively, the inductance and resistance of the motor drive winding; c_{cef} is the back electromotive force coefficient; n is the motor torque constant; l_{tf} is the tether length at the beginning of the current phase; r_c is the radius of the coil with a tether.

Based on (1-8), we now consider the features of the mathematical model of the RC in each of the phases of the abnormal conditions. In the first phase, for $U = 0, z = z_0, \dot{x} > 0$ we get:

$$m\ddot{x} = F_w - F_tcos\alpha - F_x^{a.r.}, \tag{9}$$

$$F_{pr} = F_tsin\alpha + mg, \tag{10}$$

$$\alpha = \arccos\frac{x}{\sqrt{x^2 + z_0^2}}, \tag{11}$$

$$L_c\dot{I} + R_cI = -c_{cef} * \omega_c, \tag{12}$$

$$(\mathcal{J} + mr_c{}^2)\dot{\omega_c} + \mathcal{E}\omega_c = nI + ((F_x^{a.r.} - F_w)cos\alpha + (mg - F_{pr})sin\alpha)r_c, \tag{13}$$

$$F_t = \frac{nI}{r_c}, \tag{14}$$

$$l_t = l_{ts} - r_c\int_0^t \omega_c dt, 0 < t \le t_1;\ l_t(t_1) = l_{tsafe}, \tag{15}$$

where t_1 is the time of the end of the first phase. In the second phase, at $U = U_{max}, z = z_0$, $\dot{x} > 0$:

$$m\ddot{x} = F_w - F_x^{a.r.} - F_tcos\alpha, \tag{16}$$

$$F_{pr} = F_t sin\alpha + mg, \tag{17}$$

$$\alpha = \arccos\frac{x}{\sqrt{x^2 + z_0^2}}, \tag{18}$$

$$L_c\dot{I} + R_c I = U_{max} - c_{cef} * \omega_c, \tag{19}$$

$$(\mathcal{J} + m{r_c}^2)\dot{\omega}_c + \mathcal{E}\omega_c = nI + ((F_x^{a.r.} - F_w)cos\alpha + (mg - F_{pr})sin\alpha)r_c, \tag{20}$$

$$F_t = \frac{nI}{r_c}, \tag{21}$$

$$l_t = l_{tsafe} - r_c\int_{t_1}^{t}\omega_c dt, t_1 < t \le t_2;\ l_t(t_2) = l_{tmax}, \tag{22}$$

where t_2 is the time of the end of the second phase. In the third phase, at $U = U_{in}$, $z = z_0$, $\dot{x} < 0$:

$$m\ddot{x} = F_w + F_x^{a.r.} - F_t cos\alpha, \tag{23}$$

$$F_{pr} = F_t sin\alpha + mg, \tag{24}$$

$$\alpha = \arccos\frac{x}{\sqrt{x^2 + z_0^2}}, \tag{25}$$

$$L_c\dot{I} + R_c I = U_{pr.} - c_{cef} * \omega_c, \tag{26}$$

$$(\mathcal{J} + m{r_c}^2)\dot{\omega}_c + \mathcal{E}\omega_c = nI - ((F_x^{a.r.} + F_w)cos\alpha + (mg - F_{pr})sin\alpha)r_c, \tag{27}$$

$$F_t = \frac{nI}{r_c}, \tag{28}$$

$$l_t = l_{tmax} - r_c\int_{t_2}^{t}\omega_c dt, t_2 < t \le t_3;\ l_t(t_3) = l_{tsafe}, \tag{29}$$

where t_3 is the end time of the third phase.

The choice of control voltage U_{in} in order to minimize the speed of UAV flight through point D, as analysis shows (25-29), can be done based on the ratio:

$$U_{max} > U_3 > F_w R_c r_c cos\alpha_D / n(1 - sin\alpha_D), \tag{30}$$

$$\alpha_D = \arccos\frac{x_D}{\sqrt{x_D^2 + z_0^2}}, \tag{31}$$

where x_D is the coordinate of point D; α_D is the tether angle of inclination to the horizon plane at point D.

In the fourth phase, the UAV returns to the initial point C at $z = z_0$ (Fig. 2); while the tether is wound, reaching $l_t = l_{ts}$. The law of formation of the control voltage on the drive motor U has the form:

$$U = k_{up}(l_t - l_{ts}) + k_{ud}\dot{l}_t + k_{ui}\int_{t_3}^{t}(l_t - l_{ts})dt, \tag{32}$$

$$t_3 < t \leq t_4, l_t(t_4) = l_{ts}, \tag{33}$$

where k_{up}, k_{ud}; k_{ui} are the control parameters that largely determine the dynamics of the UAV movement in the fourth phase; t_4 is the time of the end of the fourth phase.

In general, the mathematical model of the RC in the fourth phase, taking into account (32, 33), is identical to its model (23-29) in the third phase. In the fifth phase, when implementing an aperiodic UAV landing at the UGV landing place, we will form control U in the form:

$$U = U_0 + k_{lp}l_t + k_{ld}\dot{l}_t, \tag{34}$$

where U_0 is the control voltage on the TM engine, equal to its value at the end of the fourth phase; k_{lp}, k_{ld} are the control parameters.

The mathematical model of the RC in this phase when the UAV moves in the direction of the tether winding, taking into account (34), has the form:

$$m\ddot{x} = F_w - F_t cos\alpha + F_x^{a.r.}, \tag{35}$$

$$m\ddot{z} = F_{pr} - F_t sin\alpha + F_z^{a.r.} - mg, \tag{36}$$

$$\alpha = \arccos\frac{\mathrm{x}}{\sqrt{x^2 + z^2}}, \tag{37}$$

$$L_c\dot{I} + R_cI = U_0 + k_{lp}l_t + k_{ld}\dot{l}_t - c_{cef}\omega_c, \tag{38}$$

$$(\mathcal{J} + m{r_c}^2)\dot{\omega}_c + \mathcal{E}\omega_c = nI - ((F_x^{a.r.} - F_w)cos\alpha + (mg - F_z^{a.r.} - F_{pr})sin\alpha)r_c, \tag{39}$$

$$F_t = \frac{nI}{r_c}, \tag{40}$$

$$l_t = l_{ts} - r_c\int_{t_4}^{t}\omega_c dt, t_4 < t \leq t_5 ;\ l_t(t_5) = 0 \tag{41}$$

where t_5 is the time of the end of the fifth phase and the completion of the RC operation in an abnormal conditions in general.

4. MODELING THE ROBOTIC COMPLEX OPERATION IN ABNORMAL CONDITIONS

The purpose of the modeling was to verify the effectiveness of the adopted technical solutions, as well as to determine the rational parameters of the TM motor control as applied to the operation of the RC in an abnormal conditions. Modeling was carried out in accordance with models (9-41). In the modeling process, the following characteristic parameters of UAV and TM were used: $m = 6kg$; $U_{max} = 300B$; $L_c = 3 * 10^{-5}$ H; $R_c = 0.16\ om$; $c_{cef} = 0{,}016$ B/rad; $r_k = 0{,}3\ m$; $\mathcal{J} = 0{,}7\ kg/m^2$; $\mathcal{E} = 3 * 10^{-3} nm/rad$; $n = 0{,}5\ n/$A; $l_{ts} = 25\ m$; $l_{tsafe} = 30\ m$; $F_w = 30\ n$; $\rho = 12\ kg/m^3$; $c_{dz} = 1.15$: $c_{dx} = 0.12$. The rational control coefficients found in the process of modeling in the fourth and fifth phases are, respectively, $k_{up}, = 40\ V/m; k_{ud} = 35\ V/ms$; $k_{ui} = 1$B and $k_{lp} = 15.7\ V/m$, $k_{ld} = 1.5\ V/ms$, and the control voltage on the TM motor winding in the third phase is $U_{in} = 200B$.

The results of modeling the typical process of RC operation in an abnormal conditions of extreme wind exposure to UAVs are presented in Figures 3-6. The initial conditions of this process are: $x(0) = x_0 = 20\ m$; $z_0 = 15m$; $\dot{x}(0) = 0$; $\omega_c(0) = 0$. Figures (3-6) indicate the time $t_1 \dots t_5$ of the end of the corresponding phases of the process.

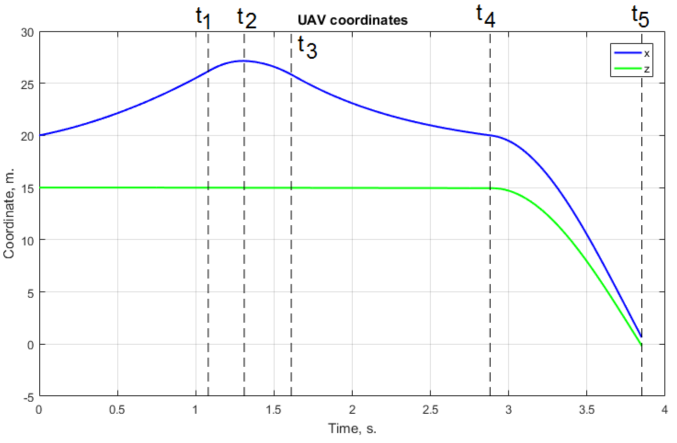

Fig. 3 – UAV x and z coordinates

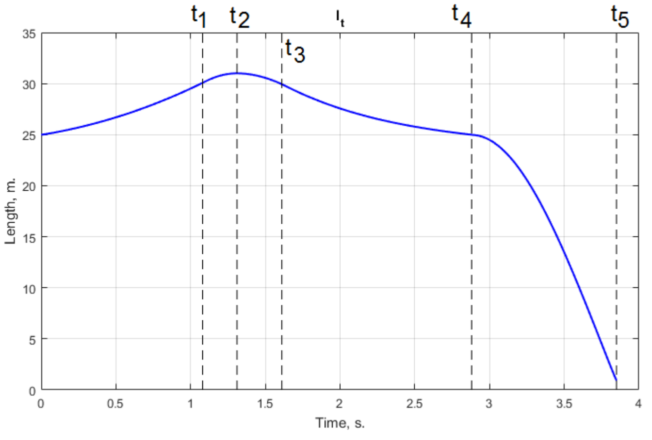

Fig. 4 – Change in tether length

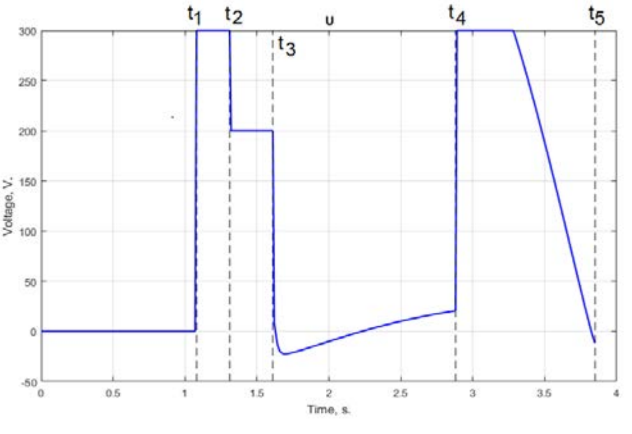

Fig. 5 – Control voltage U on the TM motor winding

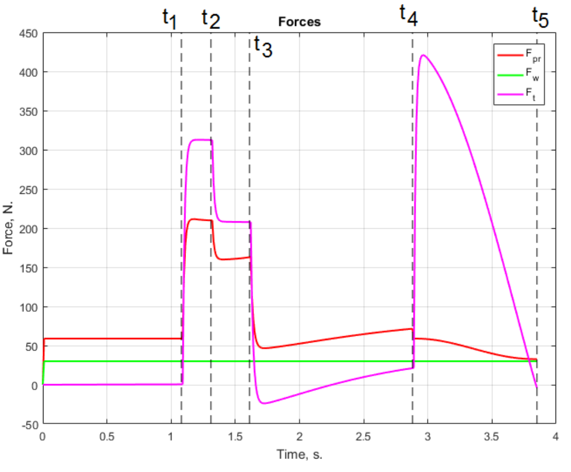

Fig. 6 – Forces applied to the UAV

It is seen that when using the adopted algorithm for the formation of the control voltage U the TM effectively operates in all phases of the abnormal conditions.

5. CONCLUSIONS

A method is proposed for implementing the procedure for through-flight (predeparture) automated inspection of the outer surface of an aircraft in its open air parking area. The hardware implementation of the method is based on the use of a robotic complex, including an unmanned aerial vehicle and an unmanned ground vehicle that are flexibly connected by a tether mechanism. A variant of the functioning of the complex in the inspection process is considered. The study of the most critical mode of operation of the complex under extreme wind actions on an unmanned aerial vehicle was carried out. It is shown that the proposed algorithm for the formation of control voltage on the drive motor of the tether mechanism ensures the prevention of collisions of an unmanned aerial vehicle with an aircraft and a soft landing of this device on the landing place of an unmanned ground vehicle.

ACKNOWLEDGMENTS

The authors would like to acknowledge the financial support from the STATUS KONSALT LLC.

REFERENCES

[1] * * * Pre-flight inspection of the aircraft. Available at: http://old.as-club.ru/kurs3/aero/html/kurs_1102_0.html
[2] D. Alonso Tabares and F. Mora-Camino, Aircraft ground handling: Analysis for automation, in *17th AIAA Aviation Technology, Integration, and Operations Conference* (pp. 16-18), Denver, 2017.
[3] * * * Robots and aviation: preflight structural inspection. Available at: http://robotrends.ru/pub/1906/roboty-i-aviaciya-predpoletnyy-strukturnyy-osmotr
[4] * * * Airbus attracted a drone to inspect aircraft. Available at: https://nplus1.ru/news/2016/07/18/airbus
[5] * * * Drone system will be used to inspect Air NZ planes. Available at: https://www.straitstimes.com/business/companies-markets/st-engineering-in-tie-ups-with-air-nz-honeywell
[6] * * * Airline testing aircraft inspection drones. Available at: https://www.avweb.com/recent-updates/unmanned-vehicles/airline-testing-aircraft-inspection-drones/

[7] L. Wang, D. Cheng, F. Gao, F. Cai, J. Guo, M. Lin and S. Shen, *A collaborative aerial-ground robotic system for fast exploration*, 2018. Available at: https://arxiv.org/pdf/1806.02487.pdf

[8] * * * Unmanned helicopter and ground robot jointly explore hazardous areas. Available at: http://www.robogeek.ru/voennaya-robototehnika/bespilotnyi-vertolet-i-nazemnyi-robot-sovmestno-issleduyut-opasnye-zony

[9] L. Cantelli, M. Presti, M. Mangiameli, C. Melita and G. Muscato, *Autonomous cooperation between UAV and UGV to improve navigation and environmental monitoring in rough environments*, At Zagreb, 2013.

[10] N. Gavrilov, *Agrotechnical complex with unmanned aerial vehicle, patent RU 2 648 696*. Available at: https://yandex.ru/patents/doc/RU2648696C1_20180328

[11] T. S. Khorev, K. S. Lelkov and V. A. Petrukhin, *Mobile wheeled robot for monitoring aerodrome infrastructure facilitie*s, Publishing House of the Moscow Aviation Institute, 2019.

[12] P. Kim, L. Price and Y. Cho, *UAV-UGV cooperative 3D environmental mapping*, Proceedings Paper Formatting Instructions, 2019.

[13] T. Miki, P. Khrapchenkov and K. Hori, UAV/UGV autonomous cooperation: UAV assists UGV to climb a cliff by attaching a tether, in *2019 International Conference on Robotics & Automation*, Montreal, 2019.

[14] C. Papachristos and A. Tzes, The power-tethered UAV-UGV team: A collaborative strategy for navigation in partially-mapped environments, in *22nd Mediterranean Conference on Control and Automation* (pp. 1153-1158), Palermo, 2014.

[15] X. Xuesu, D. Jan, and R. Robin, Murphy, autonomous visual assistance for robot operations using a tethered UAV, in *12th Conference on Field and Service Robotics*, Japan, 2019.

[16] M. Marco Nicotra, R. Naldi and E. Garone, Taut cable control of a tethered UAV, *IFAC Proceedings Volumes*, vol. **47**, no. 3, pp. 3190-3195, 2014.

[17] S. B. Modi, Comparison of three obstacle-avoidance methods for a mobile robot, *International Society for Optics and Photonics*, vol. **4572**, pp. 290-298, 2001.

[18] T. S. Khorev, *Algorithm for detecting obstacles and adjusting control points of the route of the ground wheel module*, Central Research Institute of Electrical Appliances, 2018.

[19] T. Bresciani, *Modellingm identification and control of a quadrotor helicopter*, Lund University, 2008.

[20] A. E. Guryanov, Quadrocopter control modeling, *Engineering Bulletin*, no. 8, pp. 522-534, 2014.

[21] I. I. Ogoltsov, N. B. Rozhnin and V. V. Cheval, Development of a mathematical model of the spatial flight of a quadrocopter, *Proceedings of the Moscow Aviation Institute*, no. 83, pp. 55-80, 2015.

[22] Y. Chen, D. Baek, A. Bocca, A. Macii, E. Macii and P. Massimo. (2018). *A case for a battery-aware model of drone energy consumption.* DOI: 10.1109/INTLEC.2018.8612333.

[23] B. S. Alyoshin, A. I. Chernomorsky and S. V. Feshchenko, *Orientation, navigation and stabilization of uniaxial wheel modules*, Publishing House of the Moscow Aviation Institute, 2012.

[24] K. Krayushkina, O. Prentkovskis, A. Bieliatynskyi, J. Gigineishvili, A. Skrypchenko, A. Laurinavičius, K. Gopalakrishnan and J. Tretjakovas, Perspectives on using basalt fiber filaments in the construction and rehabilitation of highway pavements and airport runways, *Baltic Journal of Road and Bridge Engineering,* vol. **11**, no. 1, pp. 77-83, 2016.